International Journal of Nanomedicine

Dovepress
open access to scientific and medical research

Open Access Full Text Article

ORIGINAL RESEARCH

Tangerine Peel-Derived Exosome-Like Nanovesicles Alleviate Hepatic Steatosis Induced by Type 2 Diabetes: Evidenced by Regulating Lipid Metabolism and Intestinal Microflora

Junju Zou[1–3,*], Qianbo Song[2,*], Pang Chui Shaw[4], Yongjun Wu[1,5], Zhong Zuo[2], Rong Yu[1,3]

[1]School of Traditional Chinese Medicine, Hunan University of Chinese Medicine, Changsha, Hunan, 410208, People's Republic of China; [2]School of Pharmacy, Faculty of Medicine, The Chinese University of Hong Kong, Hong Kong SAR, People's Republic of China; [3]Hunan Key Laboratory of Traditional Chinese Medicine Prescription and Syndromes Translational Medicine, School of Pharmacy, Hunan University of Chinese Medicine, Changsha, Hunan, 410208, People's Republic of China; [4]School of Life Sciences, The Chinese University of Hong Kong, Hong Kong SAR, People's Republic of China; [5]School of Pharmacy, Hunan University of Chinese Medicine, Changsha, Hunan, 410208, People's Republic of China

*These authors contributed equally to this work

Correspondence: Rong Yu, School of Traditional Chinese Medicine, Hunan University of Chinese Medicine, Changsha, 410208, People's Republic of China, Email yurong8072@qq.com; Zhong Zuo, School of Pharmacy, the Chinese University of Hong Kong, Hong Kong, SAR, 999077, People's Republic of China, Email joanzuo@cuhk.edu.hk

Purpose: Non-alcoholic fatty liver disease (NAFLD) represents a significant global health burden, exhibiting a strong correlation with insulin resistance, obesity, and type 2 diabetes (T2DM). Despite the severity of hepatic steatosis in T2DM patients, no specific drugs have been approved for clinical treatment of the disease. Tangerine peel is one kind of popular functional food and reported to possess hypoglycemic and lipid-lowering potential. In this study, we investigated the effects of Tangerine-peel-derived exosome-like nanovesicles (TNVs) on hepatic lipotoxicity associated with T2DM.

Methods: The TNVs was prepared by differential centrifugation of the aqueous extract of Tangerine and chemical properties were characterized using transmission electron microscopy (TEM), nanoparticle tracking analysis (NTA) and LC-MS/MS. The hypoglycemic and lipid-lowering potential of TNVs were possessed by biochemical measurement, RT-PCR, 16S rRNA sequencing, GC/MS, UHPLC-MS/MS, in vivo small animal imaging assay and HE staining. Subsequently, effects of TNVs on lipid accumulation and glycolysis were investigated on 3T3-L1 and AML-12 cells.

Results: TNVs significantly inhibited insulin resistance, reduced hepatic lipid accumulation, facilitate intestinal mucosal repair, rescued gut microbiota dysbiosis, regulated colonic SCFA and liver bile acid metabolism in *db/db* mice. Furthermore, TNVs restored the expression of key genes in glucose and lipid metabolism (ACC, AMPK, CD36, LXRα, PPAR-γ, SREBP-1) while activating the expression of genes related to glycolysis (G6Pase, GLUT2, PCK1, PEPCK) in *db/db* mice. Further cell-based mechanistic studies revealed that TNVs reduced lipid accumulation in 3T3-L1 and AML-12 cells via regulation of glucose and lipid metabolism-related genes (UCP1, FGFR4, PRDM16, PGC-1α, Tmem26, Cpt1, Cpt2 and PPAR-α).

Conclusion: We for the first time demonstrated that TNVs could significantly improve glucose and lipid metabolism via activating the expression of genes related to fatty acid β-oxidation and glycolysis.

Keywords: tangerine peel, plant-derived exosome-like nanoparticles, diabetes mellitus, metabolomics, gut microbiota, fat accumulation

Introduction

Non-alcoholic fatty liver (NAFLD) is a common complication of Type 2 diabetes mellitus (T2DM), and usually leads to hepatic lipid accumulation and inflammation. The frequent coexistence and synergistic interaction of NAFLD and T2DM exacerbated the clinical risks of hepatic and extrahepatic injury.[1] Recently researches showed that the disturbed gut-microbiota

Received: 17 May 2024
Accepted: 25 September 2024
Published: 30 September 2024

Graphical Abstract

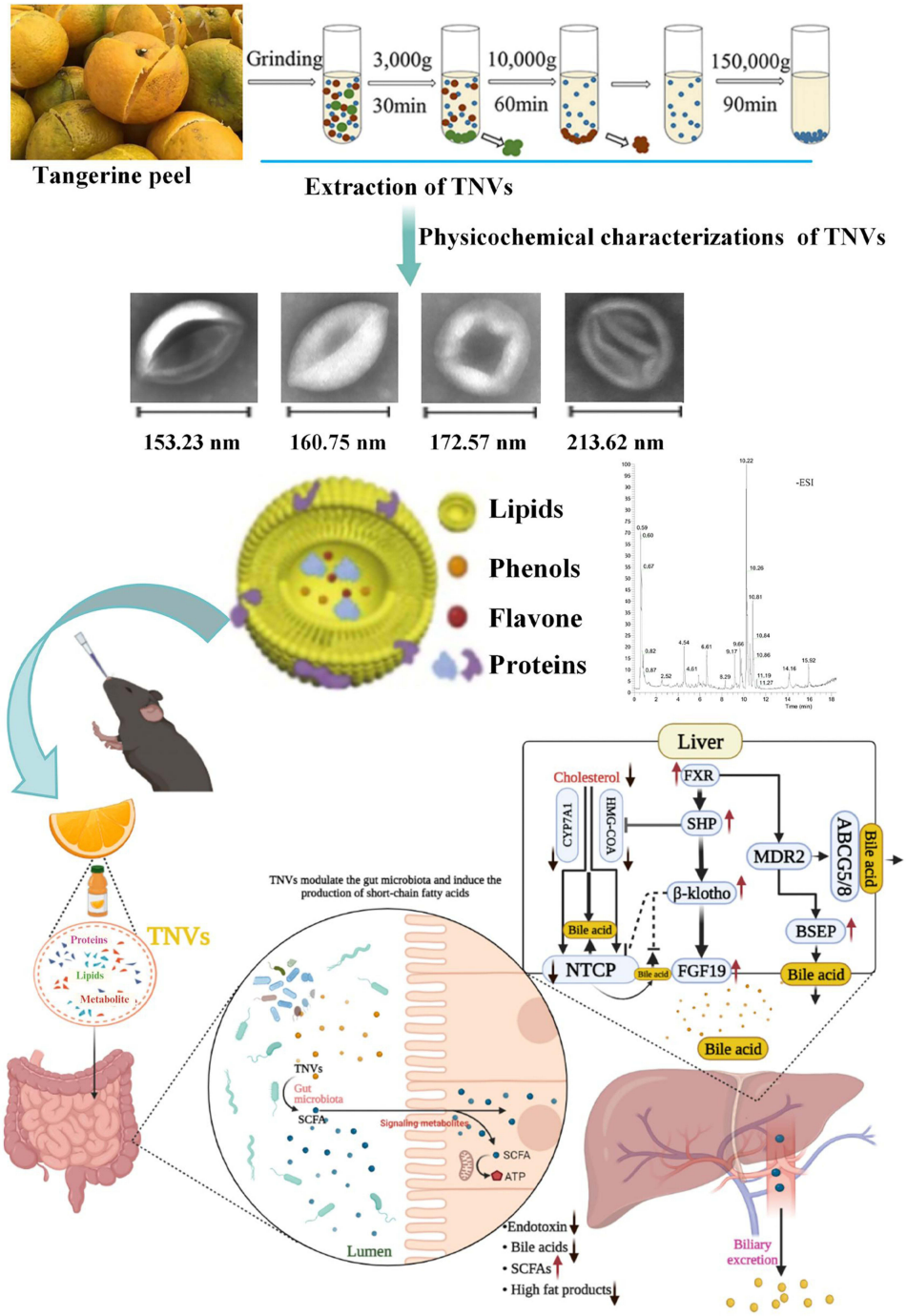

was involved in the pathogenesis and progression of T2DM and its complications.[2] Furthermore, increasing evidence suggested that metabolites produced by gut microbiota was involved in the gut-liver axis communication and ultimately contributed to the alleviation of metabolic disorders associated with T2DM-related fatty liver.[3] Therefore, restoration of the disordered gut microbiota community might be one potential therapeutic strategy to glucose and lipid metabolism diseases.

Tangerine peel (Citrus reticulatae Pericarpium, CRP; commonly known as Chenpi in Chinese) possesses medicinal and dietary properties as a traditional Chinese medicine.[4] Traditional Chinese medicine theory considered that Tangerine peel could regulate qi, invigorate the spleen, and dry dampness while resolving phlegm. The main constituents of tangerine peel included volatile oils, flavonoids, vitamins, pectin, polysaccharides, and alkaloids.[5] Modern pharmacological studies also reported that tangerine peel exhibited hepatic-protection,[6] antioxidant,[7,8] anti-inflammatory,[8] and lipid-lowering effects.[9,10] For instance, numerous epidemiological studies have demonstrated a positive correlation between the consumption of citrus flavonoids and a reduced mortality rate from cardiovascular diseases.[11–13] Previous studies showed that the medicinal value of tangerine peel was increased with its duration of storage. As the peel aged, the content of volatile oils like limonene and terpenes decreased while that of flavonoids and phenolic compounds increased.[14]

Recently, naturally occurring extracellular vesicle-like nanoparticles derived from plants, known as Plants-release Exosome-like Nanovesicles (PENs), have gained great attention for their numerous biological effect such as antioxidant, anti-inflammatory and regenerative activities.[15] Although the aqueous extracts of tangerine peel have been utilized in treating non-alcoholic fatty liver disease, [16] T2DM,[8] and other cardiovascular diseases[12] for decades, the therapeutic potential of tangerine peel-derived exosome-like nanovesicles (TNVs) on diabetes and its associated complications have not yet investigated. Herein, it was hypothesized that PENs from freshly harvested tangerine peel exhibited anti-diabetic and anti-lipidemic properties. In this study, TNVs was isolated and purified for the first time and their hypoglycemic and hypolipidemic effects in *db/db* mice was also investigated. Furthermore, an integrative analysis of hepatic metabolites, gut microbiota, and gut microbiota-derived metabolites in *db/db* mice along with evaluations of its impact on lipid accumulation in cells was conducted to gain a comprehensive understanding of the underlying pharmacological mechanisms on the hypoglycemic and hypolipidemic effects of TNVs.

Material and Methods

Reagents

Commercial fresh tangerine peel was purchased in October from Xinhui District, Jiangmen City, Guangdong Province. It was identified as *Citrus sinensis* "Xinhui Cheng", a plant belonging to the Rutaceae family, by Professor Wu Yongjun from the Department of Medicinal Botany at Hunan University of Traditional Chinese Medicine. The kits for the determination of high-density lipoprotein cholesterol (HDL-C), total cholesterol (TC), triglycerides (TG), low-density lipoprotein cholesterol (LDL-C), alanine aminotransferase (ALT) and aspartate aminotransferase (AST) were supplied by Nanjing Jiancheng Bioengineering Institute (Nanjing, China); Metformin (Sino American Shanghai Squibb Pharmaceutical Co., Ltd., approval No.:20123070); Antibodies against FITC-Phalloidin (RM02836), Claudin (A21971), Occludin (A2601) and ZO-1(A0659) were supplied by ABclonal Technology Co. Ltd., (ABclonal, Wuhan, China).

Preparation of TNVs

TNVs were isolated and extracted from tangerine peel using gradient centrifugation as described previously.[17] Briefly, fresh tangerine peel was washed with deionized water for 2 times, and mixed with 4°C phosphate-buffered saline (PBS) for 6 h. The resulting homogenate was sequentially centrifuged at 4°C, first at 3,000 × g for 30 minutes, followed by 10,000 × g for 60 minutes, to obtain the juice. The obtained supernatant was then centrifuged under 4°C at 150,000 × g for 90 minutes using a Beckman Optima ultracentrifuge (Ti70 rotor, Beckman Coulter, USA) to collect the pellet and resuspended in 1 mL of PBS in shaking water bath under 4°C overnight. The obtained TNVs were rapidly frozen in liquid nitrogen and stored at −80°C until use.

Characterization of Prepared TNVs

TEM Analysis and Zeta Potential Determination

The prepared TNVs were diluted ten times with PBS and the particle number and size of TNVs in the samples were measured using a Zeta View PMX110 instrument with 405 nm laser excitation. Particle motion was analyzed using NTA software (ZetaView8.02.28). The particle size and zeta potential of TNVs were measured as previously described.[17] Briefly, 5 μL of TNVs were dropped on a Formvar-carbon coated copper grid and air-dried followed by staining with 5 μL of uranyl acetate for 2 minutes. Excess liquid was removed and electron micrographs (Hitachi, HT-7700) were captured at 80 kV.

Chemical Components Analysis

About 100mg TNVs was thawed and then mixed with 1.0 mL of 80% methanol. After 30 seconds vortex, the mixture was sonicated for 5 minutes in an ice water bath and centrifuged (4°C,12000 rpm) for 15 minutes. To obtain the filtrate, the resulting supernatant was filtered through a 0.22 μm filter for further chemical component analysis using a UHPLC-MS system (Thermo Fisher Scientific). 5 μL sample was injected into the system, the components were separated by a Waters BEH C_{18} column (1.7 μm, 2.1 *100 mm) with a mobile phase containing water (A) and 0.1% formic acid in acetonitrile (B) at a flow rate of 0.4 mL/min under the following elution gradient program: 5– 15% B from 0 min to 3.5 min; 15–30% B from 3.5 to 6 min; 30%~30% B from 6 to 6.5 min; 30% ~70% B from 6.5 min to 12 min; 70–70% B from 12 min to 12.5 min; 70–100% B from 12.5 min to 18 min.

To characterize the molecular constituents of the exosomes, including proteins, RNA, and lipids, polyacrylamide gel, agarose gel, and thin-layer chromatography (TLC) were utilized to detect proteins, RNA, and lipids, respectively.[18] Subsequent to the electrophoresis, proteins within the gel matrix were visualized using Coomassie brilliant blue staining. Lipid extraction from the exosomes was performed utilizing the Folch method, followed by their resolution on silica gel TLC plates. Detection and visualization of the lipid fractions were achieved by staining with a 10% copper sulfate solution in an 8% phosphoric acid matrix.

Intestinal Absorption and Biodistribution of TNVs

Intestinal Uptake of TNVs Investigated by VoLo and AML-12 Cells

TNVs (200 μg/mL) were incubated with 5 μM PKH-26 for 30 minutes, then centrifuged at 100,000 × *g* for 1 h. The pellet was collected and resuspended in 200 μL of PBS followed by 24-hour incubation with VoLo cells or AML-12 cells. The cell cytoskeleton and nuclei of VoLo cells and AML-12 cells were subsequently stained with FITC–phalloidin and DAPI, respectively, for further observation on the potential uptake of TNVs into VoLo cells and AML-12 cells with a fluorescence microscope (Leica, STELLARIS, Germany).

Biodistribution of Orally Administrated TNVs

At 24 h post oral bolus dose of 200 mg/kg TNVs labeled with DiR fluorescent dye in C57 BL/Ks mice (n = 3), the biodistribution of TNVs in the mice was imaged via IVIS Lumina system (Perkin Elmer). Then the mice were anesthetized with isoflurane to collect their small intestine, colon, liver, kidney, spleen, pancreas, and heart for further analyses of DiR fluorescence signals.

Evaluation on the Anti-Hyperglycemic and Anti-Lipid Accumulation Effects of TNVs

Animal Model and Treatment

Seven-week-old male C57BL/Ks mice and seven-week-old male C57BL/KsJ-*db/db* mice (*db/db* mice) were supplied by Hunan Silk Laboratory Animal Co., Ltd. All procedures were consistently conducted in strict compliance with the Guidelines for the Use of Laboratory Animals of the National Institutes of Health of the United States of America. The Hunan University of Chinese Medicine Institutional Review Board reviewed and approved the study protocol before its initiation (Ethics number: SJA2022184). The animals were maintained under standard environmental conditions (22°C temperature with a humidity of 50 ± 5%), with a 12-hour light/dark cycle. Mice were divided into four groups (n = 6 per group): normal control group, T2D model group, positive control group, and TNVs treatment group. The normal control group (Control) consisting of C57 BL/Ks mice was treated with physiological saline. The three groups of male db/db mice were administered treatments as follows: the TNVs treatment group received 200 mg/kg TNVs (TNVs group), the positive control group received 250 mg/kg metformin (Met group), and the T2D model group received the vehicle (Model group). After an 8-week oral treatment, the mice were anesthetized with isoflurane. Blood samples were quickly taken, followed by the collection of liver, colon, and feces samples for further molecular studies. The liver of each animal was weighed at the end of the experiment to calculate the liver index: liver weight/body weight × 100%.

Anti-Hyperglycemic Effects of TNVs

A weekly blood collection was conducted via the tail vein of the mice to monitor their fasting blood glucose (FBG) levels using a glucometer. At the end of 8th week, intraperitoneal glucose tolerance tests (ipGTT, 2 g/kg) and intraperitoneal insulin tolerance tests (ipITT, 1 IU/kg) were performed as described by us before.[19] The AUC of blood glucose levels at various time points (0, 30, 60, 90, and 120 min) was computed using data from all points for each individual animal was detected on the third day. Serum insulin (INS) levels were measured using an enzyme-linked immunosorbent assay (ELISA) kit (Elabscience Biotechnology Co., Ltd, CN). Serum fasting insulin levels on Day 17 were also determined using an enzyme-linked immunosorbent assay (ELISA) kit (Elabscience Biotechnology Co., Ltd). Homeostatic model assessment for insulin resistance (HOMA-IR) was calculated as FBG (mM/L) × FINS (mU/L)/22.5.

Anti-Lipid Accumulation Effects of TNVs

Serum Biomarkers Analyses

The blood samples were centrifuged (3500 rpm, 30 min, 4°C) and the levels of TG, TC, HDL-C, and LDL-C were measured using the corresponding ELISA kits (Elabscience Biotechnology Co., Ltd, CN). In addition, serum levels of the liver function indicators, including ALT and AST, were also detected using their corresponding ELISA kits purchased from the Nanjing Jiancheng Bioengineering Institute (Nanjing, China).

Liver Metabolomics Analyses Using LC/MS-MS

Around 100 mg of liver sample were thawed at 4°C followed by extracting with a pre-cooled solution containing methanol, acetonitrile, and water at a ratio of 2:2:1 (v/v/v). After vortex, the mixture was sonicated for 30 min at 4°C followed by centrifugation (14,000 × g, 4°C) for 20 min. About 2 μL of the obtained supernatant was injected into UHPLC (Vanquish, Thermo Fisher Scientific) system and Orbitrap Exploris 120 mass spectrometer (Orbitrap MS, Thermo Fisher Scientific) for analysis. The components were separated via an HILIC column (2.1 mm × 100 mm, waters, Ireland) that was maintained at 25°C with a mobile phase consisting of solution A (25 mm ammonium acetate +25 mM ammonia) and solution B (acetonitrile) at a flow rate of 0.3 mL/min under a gradient elution program: 98% ~98% B, from 0 to 1.5 min; 98% B ~ 2% B, from 1.5 to 12 min; 2–2% B, from 12 to 14 min.

Liver Bile Acids Analyses Using LC/MS-MS

To evaluate the bile acid levels, 25 mg liver tissue sample from each mouse was homogenized with 1 mL H_2O for 4 min at 40 hz and sonicated for 5 min in the ice water bath. After centrifugation (5000 rpm, 4°C) for 20 min, the supernatant was transferred (0.8 mL) into a 2 mL EP tube with 0.2 mL of methanol (contains 0.10 μM of CA-D4, UDCA-D4, and LCA-D4 used as the internal standard). Injected bout 2 μL of the obtained supernatant into UHPLC-MS system for LC-MS/MS analysis of 70 bile acids as described previously by Xie et al.[20]

mRNA Level Detection

A total RNA isolation kit (Foregene, Chengdu, China) was utilized to extract RNA from liver samples (25 mg) obtained from each mouse, following the manufacturer's protocol.[21] Subsequently, cDNA was amplified in accordance with the following parameters: an initial denaturation at 95°C for 3 minutes; then, 40 cycles of denaturation at 95°C for 5 seconds, followed by extension at 65°C for 30 seconds. The GAPDH gene was utilized as a reference gene for normalization purposes, and the resulting data underwent statistical analysis using the $2^{-\Delta\Delta Ct}$ method, with the primer sequences specified in Table S1.

Pathological Analyses of Liver and Colon Tissue

Approximately one-quarter of the liver and colon specimens from three mice were fixed in 4% paraformaldehyde, embedded in paraffin, and subjected to hematoxylin and eosin (H&E) staining, Masson's trichrome (Jiancheng, Nanjing, China), Periodic Acid-Schiff (PAS) and Alcian blue-periodic acid-Schiff (AB-PAS).

Analysis of Gut Microbiota and Its Metabolites After Oral Administrations of TNVs

Fecal 16S rRNA Sequencing

The total fecal DNA was extracted from 100 mg fecal samples by CTAB/SDS method.[22] The DNA concentration and purity were then evaluated on 1% agarose gels. Based on these concentration measurements, the DNA was diluted to 1 ng/μL with sterile water. The isolated DNA was then subjected to polymerase chain reaction (PCR) amplification via targeting the V4 region of the 16S rRNA using barcode-specific primers (forward: GTGCCAGCMGCCGCGGTAA; reverse: GGACTACHVGGGTWTCTAAT). Following amplification, the products of polymerase chain reaction were quantified by means of 2% agarose gel electrophoresis and purified. Following purification, a sequencing library was constructed using the TruSeq DNA PCR-Free Sample Preparation Kit from Illumina in the United States. The NovaSeq6000 platform was employed to generate paired-end reads through the process of sequencing.

Detection of SCFA in Fecal Samples by GC-MS/MS

The concentrations of short-chain fatty acids (SCFAs) were determined in accordance with the methodology described in the previous study.[20] The procedure commenced with the suspension of approximately 50 mg of fecal matter in 0.5 mL of Milli-Q water. This was followed by homogenization, which was conducted three times (at 6500 rpm for 20 seconds each time) with an interval of 10 seconds between each round. This was achieved using an HF-24 homogenizer (Hefan Instrument), which was equipped with 1.0 mm-diameter zirconium oxide beads. The homogenate was then centrifuged at 15,000 rpm for 10 minutes. A total of 400 μL of the supernatant was collected and mixed with 40 μL of an internal standard (5 mm N-methyl-N-trimethylsilyl). Subsequently, 40 μL of 5 M HCl was added to acidify the solution, followed by the addition of 480 μL of anhydrous diethyl ether to extract SCFAs. The resulted mixture was then cooled on ice for 5 minutes and centrifuged (10,000 g, 4°C) for 5 min. About 200 μL of the diethyl ether layer was collected and kept in a new microtube containing anhydrous Na_2SO_4 for 2 hours. After a 2-minute centrifugation (3000 g, 4°C), 2 μL supernatant was injected into SHIMADZU GC2030-0P2020-NX gas chromatography-mass spectrometer (GC-MS) coupled with a HP-FFAP capillary column (30 m, 250 μm × 0.25 μm). The standard mixture including acetic acid, propionic acid, butyric acid, isobutyric acid, and isovaleric acid were diluted into different concentrations (0.2–10 mg/mL) to plot the standard curve.

Detection of Intestinal Mucosal Barrier Proteins (Occludin, Claudin and ZO-1) Expression by Immunofluorescence Staining

The colon tissues were fixed in 4% paraformaldehyde and embedded in paraffin. Then, the tissue sections were dewaxed and dehydrated. Fully immerse the sample in 0.01 M citrate buffer (pH 6.0), and heat repair in a microwave at low heat. Wash three times with PBST, seal with 5% goat serum in a 37°C incubator for 10 minutes, then wash three times with PBST. The slides were incubated with primary antibody (1:200) overnight at 4°C. After washing three times with PBST buffer, the secondary antibody was added for incubation in the dark environment at room temperature for 1 hour. Then the secondary antibody was removed and washed three times with PBST buffer. The DAPI working solution was added on the slides prior to incubation at dark environment for 10 minutes. After washing with PBST buffer and the addition of anti-fluorescence quenching reagent, the image signal was observed and captured under a fluorescence microscope (BX53, Olympus).

Further Mechanistic Study of Anti-Lipid Accumulation and Glycolysis of TNVs in AML-12 and 3T3-L1 Cell Models

Anti-Lipid Accumulation Effect of TNVs in Hepatocyte (AML-12) Cells

AML-12 cells were cultured with DMEM media containing 10% FBS. When the AML-12 cell reached 90% confluence, they were plated at a density of 1×10^4 cells per well in 6-well plates. After 24 hours, the cells were treated with 250 μM palmitate acid (PA). For the TNVs group, cells were treated with 200 μg/mL TNVs for 24 hours and metformin (500 μM) as a positive control. After 24 hours, the cells were collected for RT-PCR detection of UCP, CEBPA, LXR-*α*, SREBP-1*c*, and ACC mRNA levels (Table S1). AML-12 cells were obtained from Procell Life Science&Technology Co., Ltd.

Anti-Glycolysis of TNVs in Adipocyte-3T3-L1 Cells

3T3-L1 cells were cultured (37°C, 5% CO_2) with DMEM medium. Upon reaching 100% confluency, the culture medium was replaced with medium containing the following components: 0.5 mm 3-isobutyl-1-methylxanthine, 1 μM dexamethasone, and 4 μg/mL insulin, with the addition of 10% FBS and 1% P/S. Then the cells were treated with DMEM containing 10% FBS, 1% P/S, and 5 μg/mL insulin for two days to induce initial differentiation of fused adipocytes. After a two-day treatment, the cells were cultured for a further day in a medium containing DMEM, 10% FBS, and 5 μg/mL insulin. The fused cells were treated with 200 μg/mL TNVs and metformin (500 μM) for 24 hours, and then the cells were collected for RT-PCR detection of FGF19, PRDM16, PGC1α, UCP1, Cidea, Cox7a1, and Tmem26 mRNA levels with their primers shown in Table S1. 3T3-L1 cells AML-12 cells were obtained from Procell Life Science&Technology Co., Ltd.

Statistical Analyses

Data were expressed as means ± SE mean (SEM). One-way analysis of variance (ANOVA) and Mann–Whitney *U*-test were used to compare the difference among different groups with $p < 0.05$ considered to be statistically significant.

Results

Preparation and Characterization of TNVs

TNVs were extracted from fresh tangerine peel juice using continuous differential centrifugation as shown in Figure 1A. As depicted in Figure 1B, the purification concentration of TNVs was approximately 1.6×10^{11} particles/mL with an average diameter of 172.1 ± 3.7 nm. The zeta potential was about −12.26 ± 4.05 mV. TNVs exhibited a spherical vesicle morphology formed by characteristic lipid bilayers (Figure 1C). TLC data showed that TNVs contained multiple types of lipids (Figure 1D). The presence of RNAse confirmed that TNVs contained RNA, mainly distributed in the molecular weight range of 100–500 bp (Figure 1E). In addition, SDS-PAGE analysis showed that the size range of proteins within

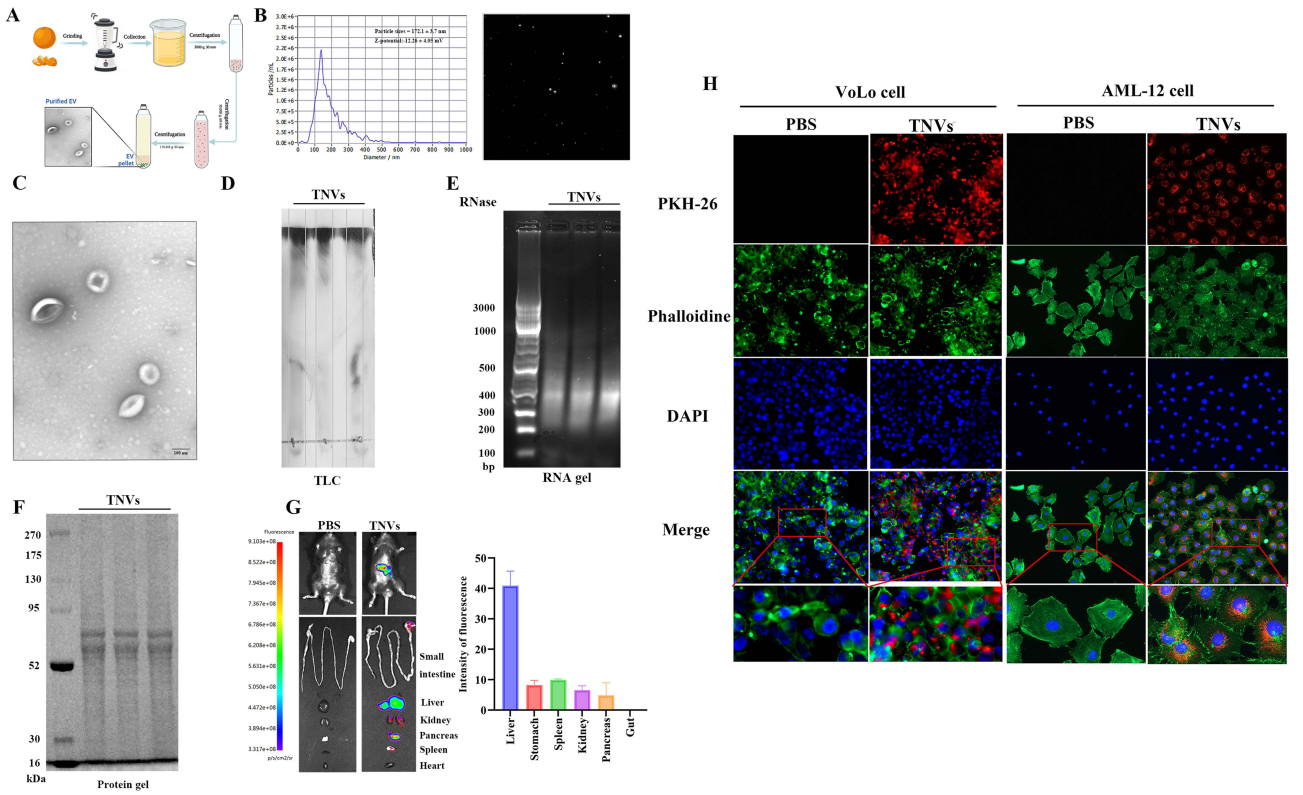

Figure 1 Physicochemical characterizations *and* in vitro/*in vivo* uptakes of TNVs. (**A**) Extraction process of TNVs. (**B**) Size distribution. (**C**) Transmission Electron Microscopy (TEM) image. (**D-F**) lipids, nucleic acids, and proteins in TNVs. (**G**) In vivo biodistribution of TNVs. (**H**) In vitro cellular uptake of TNVs.

TNVs was 16–72 kDa (Figure 1F). Therefore, nanoparticle-scaled PENs extracted from tangerine peel contained RNAs, proteins, and lipids.

To visualize the in vivo tissue distribution of orally administered TNVs, DiR-labelled TNVs were prepared and utilized for in vivo biodistribution studies. Twenty-four hours post oral administration, the DiR fluorescence signal was primarily detected in the liver while the fluorescence signal detected in the spleen, kidney, pancreas, and gastrointestinal tract were quite weak (Figure 1G). To estimate the uptake of TNVs in the intestine and liver, VoLo cells (human colorectal cancer cells) and AML-12 cells (normal mouse liver cells) were incubated with TNVs for 24 hours and found that TNVs could be taken in both cells as demonstrated in Figure 1H. Since Tangerine peel was rich in active small molecular components such as polyphenols, flavonoids, alkaloids, and essential oils, a qualitative analysis of these active small molecules in TNVs was conducted using UHPLC-QE-MS. The identification was conducted based on the mass spectrum of the sample and in accordance with the natural products mass spectrometry database and pertinent literature, as illustrated in Figure 2A and Table S2. A total of 148 compounds with high abundance were identified from TNVs. The detected molecules can be roughly divided into six main categories including terpenoids, phenylpropanoids, flavonoids, phenols, alkaloids, and amino acid derivatives (Figure 2B).

Improved insulin resistance, glucose tolerance and restored the intestinal mucosal barrier of *db/db* mice by orally administered TNVs

The hypoglycemic effect of TNVs was investigated on *db/db* mice as shown in Figure 3. Compared with the control group, the liver index (liver weight/body weight × 100%), FBG, food intake, fasting insulin level, and Homeostatic Model Assessment for Insulin Resistance (HOMA-IR) index of *db/db* group was increased ($p < 0.01$). After treatment with TNVs, the liver index, blood glucose, body weight, HOMA-IR index, food intake, and insulin levels in *db/db* mice were reduced significantly (Figure 3A–G).

The H&E staining results of colon showed that the colonic villi of mice from control group were neatly arranged with uniform distribution of intestinal glands while a large amount of degenerated glandular epithelial cells were observed in the colon of mice from *db/db* group. After treatment with TNVs, the intestinal villi of mice from TNVs group were arranged orderly with the alleviation on degeneration and swelling of glandular epithelial cell (Figure S1.A). AB-PAS staining demonstrated that the integrity of intestinal structures in mice from *db/db* group was disrupted with a notable reduction in the number of goblet cells compared with those in Control group while TNVs treatment could increase the number of goblet cells (Figure S1.B, D). Further immunofluorescence analysis revealed that the fluorescent expression of Claudin-1, ZO-1, and Occludin were significantly reduced in the colonic tissues of *db/db* mice in comparison with healthy mice while TNVs treatment could reverse the trend with the markedly enhanced fluorescence intensity of Claudin-1, ZO-1, and Occludin in the colonic tissues (Figure S1.C). In addition, the lengths of villi and crypt depths in the mouse colons were measured as well. The result indicated that both the villus height and crypt depth were increased significantly in the mice from TNVs group compared to *db/db* group (Figure S1.D).

Improved liver function, reduced blood lipids and reduced liver lipid accumulation by orally administered TNVs via reducing liver adipogenic factors and bile acids accumulation

To evaluate the effect of TNVs on lipid regulation in the liver of *db/db* mice, histological examination of hepatic tissue for lipid damage was conducted using H&E staining, Masson staining, and PAS staining. Conspicuous macrovesicular steatosis and glycogen accumulation in the liver of *db/db* mice was observed along with a slight formation of collagen fibers. After treatment with TNVs, the size of lipid droplets in the liver was reduced with decreased glycogen accumulation and absence of collagen fibers as shown in Figure 4A–C. Furthermore, after treatment with TNVs, the serum lipid levels in *db/db* mice were improved significantly with decreased serum level of TG, TC, ALT, AST, and LDL-c as well as the increased serum level of HDL-c and GSH-PX (Figure 4D).

To further reveal the potential mechanisms of hepatic lipid metabolic disorder in *db/db* mice, metabolomic analysis was employed to analyze liver samples to discover the metabolites involving in the regulation on hepatic lipid metabolic

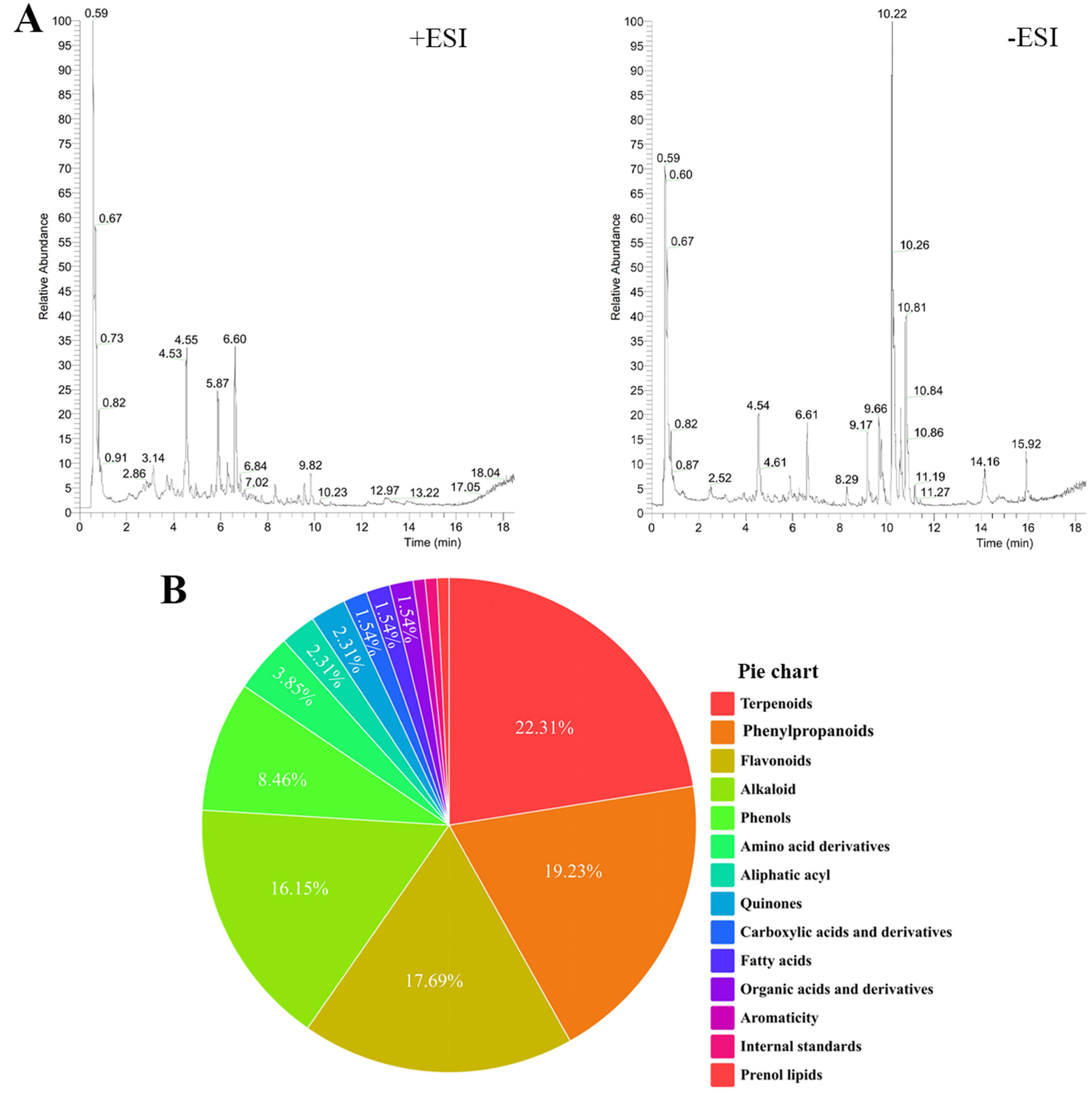

Figure 2 Mass spectrometry of TNVs. **(A)** Total ion chromatogram (+ESI and -ESI). (**B**) Pie chart with a summary of chemical components in TNVs.

disorder. Principal Component Analysis (PCA) showed significant differences among Control, TNVs and *db/db* group, indicating substantial disparities in the metabolites among them (Figure 5A and B). A total number of 2206 metabolites were identified, of which 505 showed significant variations between three groups. These distinctive metabolites could be categorized into organic acids and derivatives (16.33%) lipids and lipid-like molecules (41.22%) organic heterocyclic compounds (8.57%) organic oxides (8.98%), nucleosides and their analogs (8.16%) (Figure 5C and D). The differential metabolites between the TNVs and *db/db* groups were shown in Figures 5E and F. The chord plot of differential metabolites provides a clearer visualization of material classification and quantity changes (Figure 5G). Subsequently, 505 differential metabolites were identified (Supplementary data) and their specific functions were annotated. Through KEGG analysis, 15 pathways were annotated, among which five pathways, namely purine metabolism, arachidonic acid

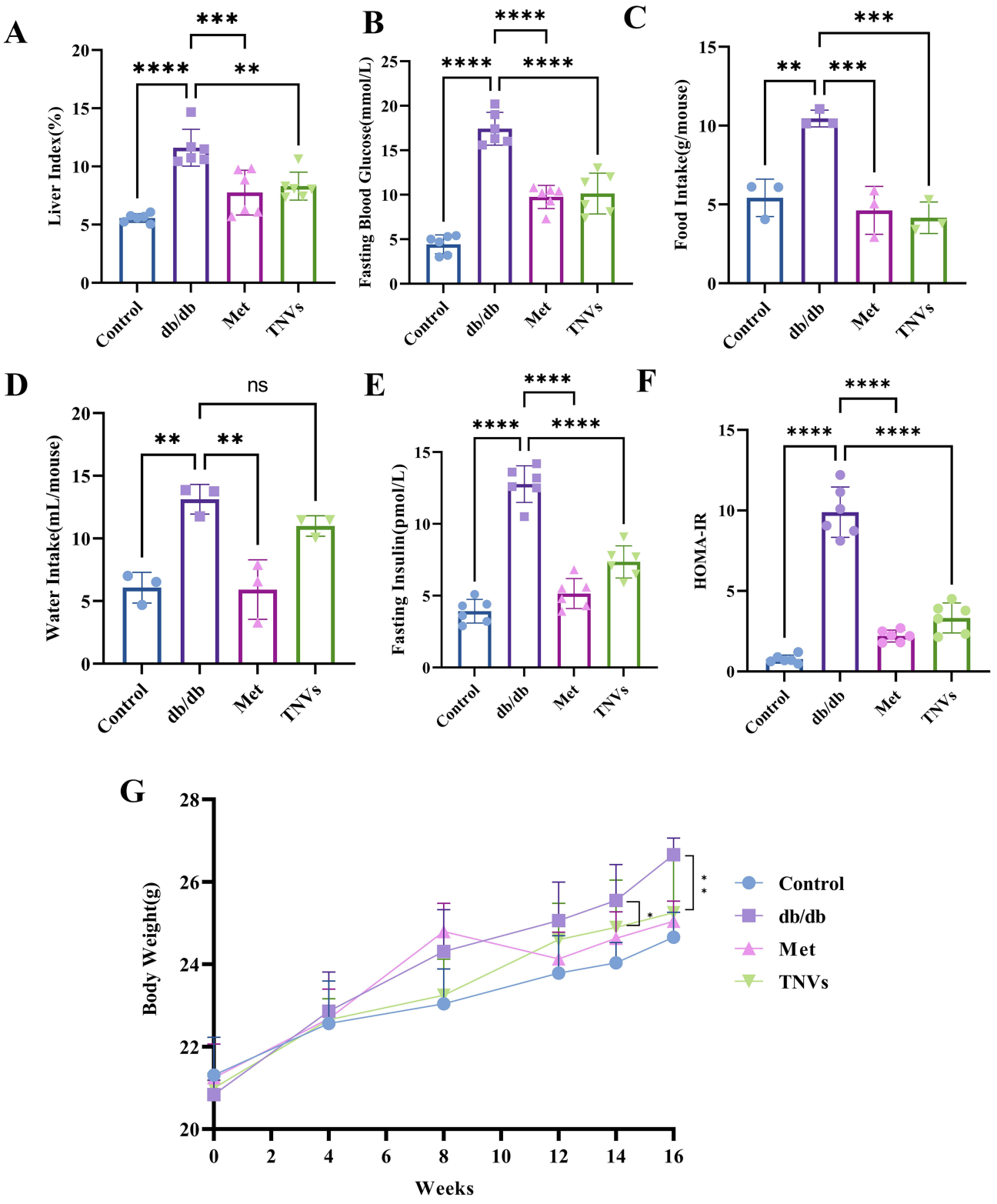

Figure 3 Effect of 200 mg/kg TNVs on biochemical parameters. (**A**) Liver index. (**B**) Fasting Blood Glucose. (**C**) Food intake. (**D**) Water intake. (**E**) Fasting insulin. (**F**) Homeostatic Model Assessment for Insulin Resistance (HOMA-IR) and body weight (**G**) of *db/db* mice. Results are expressed as means ± SEM. n=6, compared with the *db/db* group, *$p < 0.05$, **$p < 0.01$, ***$p < 0.001$, ****$p < 0.0001$.

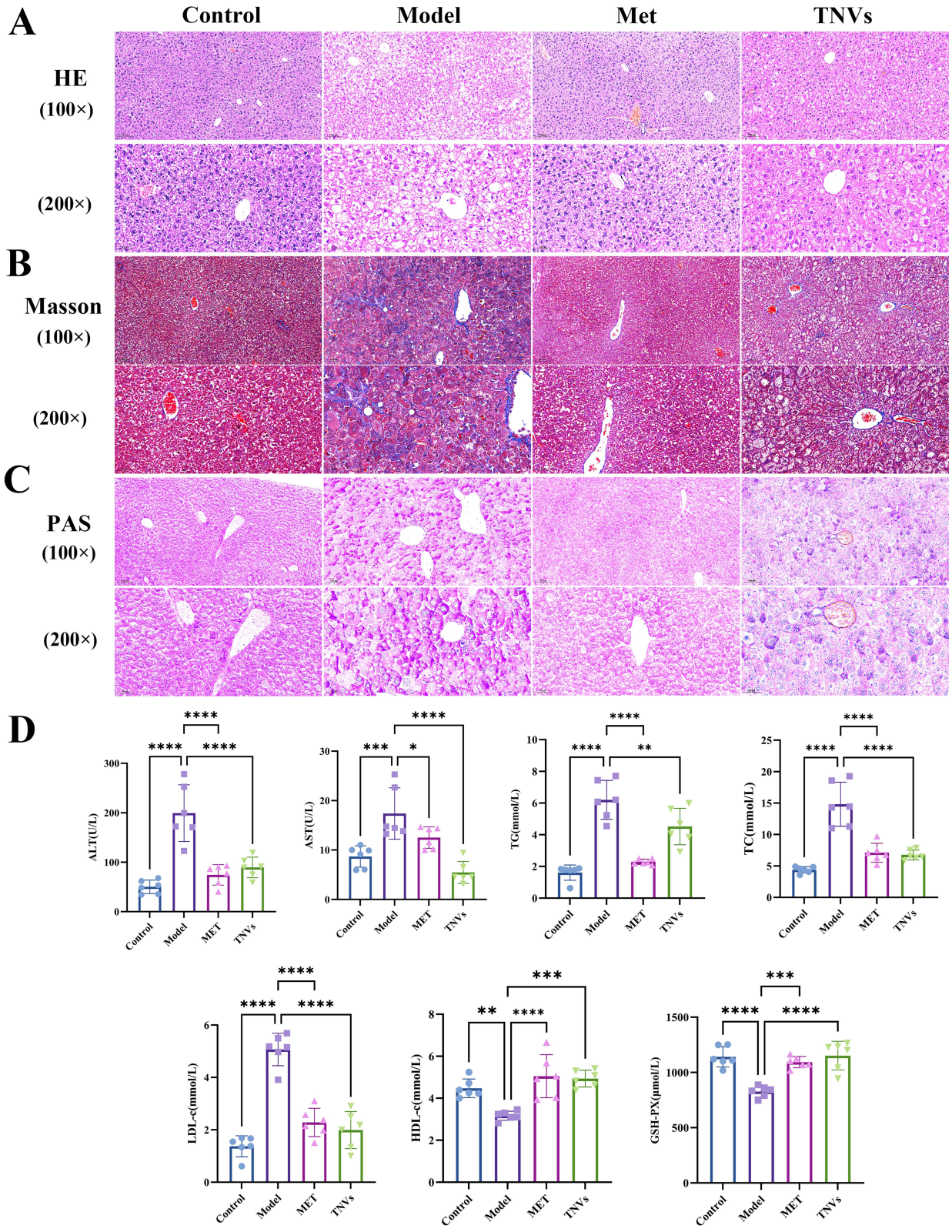

Figure 4 Impact of TNVs on hepatic lipid levels in *db/db* mice. (**A**) H&E staining of liver. (**B**) Masson staining of liver. (**C**) Periodic Acid-Schiff stain of liver. (**D**) Serum levels of ALT, AST, TG, TC, LDL-c, HDL-c and GSH-PX in *db/db* mice. Results are expressed as means ± SEM. n = 6, compared with the *db/db* group, *$p < 0.05$, **$p < 0.01$, ***$p < 0.001$, ****$p < 0.0001$.

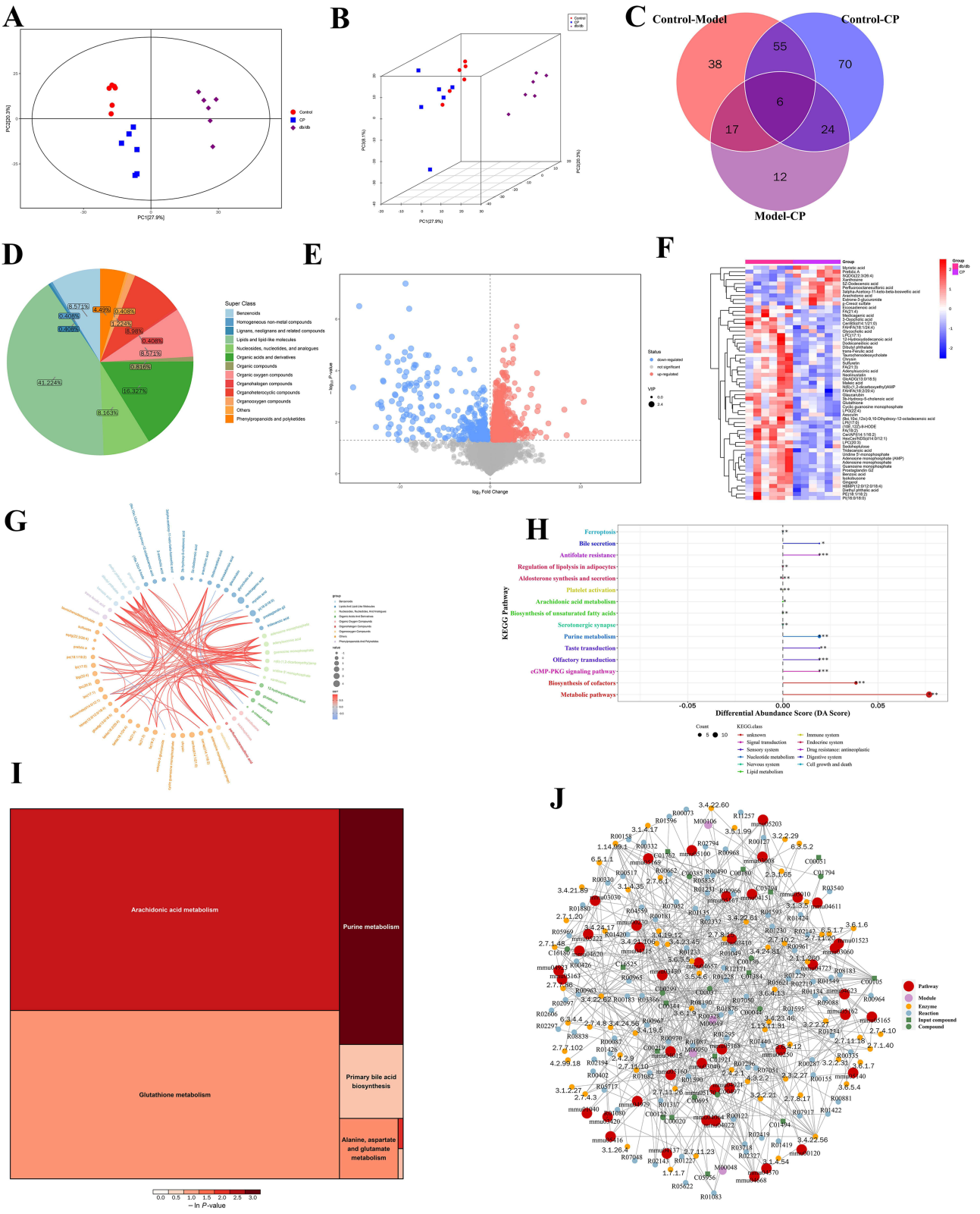

Figure 5 Liver metabolomic analyses of *db/db* mice after oral administration with 200 mg/kg TNVs. (**A**) PCA scatter plot of the metabolite profile. (**B**) The Orthogonal Partial Least Squares Discriminant Analysis (OPLS-DA) score graph. (**C**) Venn Diagram of Control, *db/db* and TNVs group. (**D**) Classification and proportion of liver metabolites. (**E**) Volcano plot of *db/db* and TNVs group. (**F**) Heat map of hierarchical clustering analysis *db/db* and TNVs group. (**G**) Chord diagram. (**H**) Differential abundance scores. (**I**) Pathway analysis diagram. (**J**). Regulatory network analysis diagram.

metabolism, glutathione metabolism, amino acid metabolism and primary bile acid biosynthesis were associated with hepatic steatosis (Figure 5H–J).

Hepatic steatosis is a pathological state with an over-accumulation of lipids in the liver. In this study, metabolomic analysis indicated that the lipid metabolic disorder in *db/db* mice was associated with hepatic steatosis. To clarify the molecular mechanisms of TNVs on lipid regulation, the key genes implicated in glycolysis, lipid metabolism, and FAO in the hepatic tissues were investigated firstly. Compared with the control group, there was a notable increase in the hepatic expressions of key glycolysis genes phosphoenolpyruvate carboxykinase (PEPCK), Glucose-6-Phosphatase (G6Pase), and phosphoenolpyruvate carboxykinase 1 (PCK1) in *db/db* mice, whereas the expression of glucose transporter 2 (GLUT2) was significantly reduced (Figure S2.A). Meanwhile, the expressions of critical lipogenesis genes such as sterol regulatory element binding transcription factor 1 (SREBP-1c), CD36, acetyl-CoA carboxylase (ACC), liver X receptor α (LXR-*α*), peroxisome proliferator activated receptor *γ* (PPAR-*γ*), and CCAAT enhancer binding protein *α* (CEBP*α*) were significantly increased (Figure S2.B). Conversely, the levels of key genes associated with fatty acid *β* -oxidation including carnitine palmitoyltransferase 1a (CPT1), carnitine palmitoyltransferase 2a (CPT2), fibroblast growth factor receptor 4 (FGFR4), PPARG coactivator 1 *α* (PGC-1*α*), transmembrane protein 26 (Tmem26), peroxisome proliferator activated receptor *α* (PPAR-*α*), uncoupling protein 1 (UCP1), and PR domain containing 16 (PRDM16) were markedly decreased (Figure S2.C). Additionally, treatment with TNVs significantly increased the expression of key genes for FAO while the levels of key genes associated with glycolysis and lipogenesis were markedly reduced (Figure S2.A-C).

Given the significant effect of TNVs on improving hepatic lipid accumulation in vivo and their ability to reduce hepatocyte lipid accumulation in *db/db* mice, the impact and molecular mechanism of TNVs on adipocyte browning and lipid deposition was further explored in 3T3-L1 cell and AML-12 cell, respectively. As demonstrated in Figure S3.A and B, it was observed that the generation of lipid droplets was significantly increased in AML-12 cells post-PA treatment and 3T3-L1 cells post-adipocyte differentiation in Oil Red O staining. However, TNVs intervention could significantly inhibit the accumulation of lipid droplets in cells. To investigate the molecular mechanism of TNVs on PA-induced hepatocyte lipid accumulation, the expression of key lipogenesis genes was quantified by RT-PCR. As shown in Figure S3.C, after treatment with TNVs, the levels of lipogenesis genes including CD36, fatty acid synthase (FASN), liver X receptor *α* (LXR-*α*), PPAR-*γ*, and SREBP-1c in PA-induced AML-12 cells were reduced significantly. The levels of lipogenesis factors including LXR-α, FASN, LPAATθ, diacylglycerol O-acyltransferase 1 (DGAT1), LIPIN1, and SREBP-1c in adipocyte-differentiated 3T3-L1 cells were reduced significantly as well (Figure S3.D). To assess the effect of TNVs on energy expenditure of adipocyte-differentiated 3T3-L1 cell, the key genes associated with FAO were also analyzed. The results revealed that TNVs treatment significantly increased the expression of key genes for FAO including Cidea, Cox7a1, PGC-1α, Prdm16, Tmem26, and UCP1 (Figure S3.E). In summary, these findings in 3T3-L1 and AML-12 cells suggested that TNVs could inhibit intracellular lipid accumulation, reduce lipogenesis and enhance energy expenditure.

Further analysis of hepatic bile acids revealed that the levels of primary/secondary bile acids including Cholic acid (CA), Allocholic acid (ACA), Dehydrocholic acid (DHCA), Glycocholic acid (GCA), Glycolithocholic Acid-3-Sulfate (GCA-3S), Hyodeoxycholic acid (HDCA), Taurolithocholic acid (TLCA), Ursodeoxycholic acid (UDCA), Chenodeoxycholic acid (CDCA), and Tauroursodeoxycholic acid (TUDCA) were significantly decreased after treatment with TNVs compared with those in *db/db* mice (Figure 6A-C). Excessive accumulation of bile acids in the liver was involved in the insulin resistance and hepatic steatosis.[23] It has been reported that FXR, small heterodimer partner (SHP), fibroblast growth factor 19 (FGF19), and β-Klotho played pivotal roles in inhibiting bile acid synthesis.[21] Compared with the Control group, *db/db* mice exhibited significantly decreased mRNA levels of FXR, SHP, FGF19, and β-Klotho while TNVs could significantly reverse the tendency (Figure 6D) by further inhibiting the expression of key genes related with bile acid uptake such as Na+/taurocholate cotransporting polypeptide (NTCP), CYP7A1, and 3-hydroxy-3-methylglutaryl-coenzyme A (HMG-COA) (Figure 6E), and promoting the expression of bile acid/cholesterol efflux genes including multidrug-resistance transporter mdr2 (MDR2), bile salt export pump (SBEP), ATP binding cassette subfamily G member 5 (Abcg5), and ATP binding cassette subfamily G member 8 (Abcg8) (Figure 6F). These results indicated that TNVs could regulate the biosynthesis, metabolism, and transport of bile acids in the liver and maintain the metabolic balance of bile acids in the hepatic system.

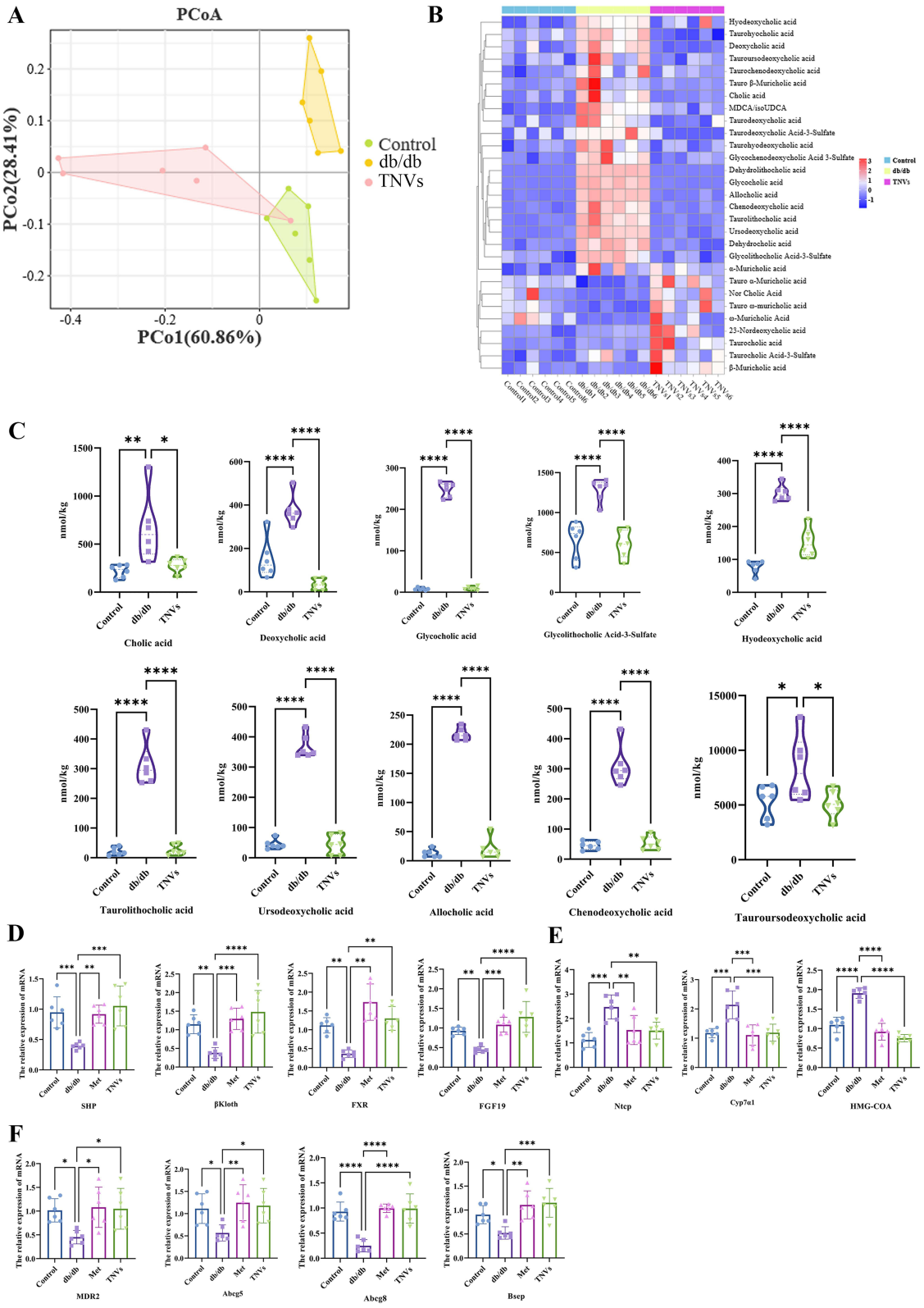

Figure 6 Effect of TNVs on bile acid metabolism and biosynthesis in liver of *db/db* mice. (**A**) PCA analysis of bile acids. (**B**) Cluster analysis of bile acids. (**C**) The levels of Cholic acid, Allocholic acid, Dehydrocholic acid, Glycocholic acid, Glycolithocholic Acid-3-Sulfate, Hyodeoxycholic acid, Taurolithocholic acid, Ursodeoxycholic acid, Chenodeoxycholic acid, and Tauroursodeoxycholic acid. (**D**) The levels of FXR, SHP, FGF19, and β-Klotho mRNA expression. (**E**) The levels of NTCP, CYP7A1, and HMG-COA mRNA expression. (**F**) The levels of MDR2, BSEP, ABCG5, and ABCG8 mRNA expression. Results are expressed as means ± SEM. n=6, compared with the *db/db* group, *$p < 0.05$, **$p < 0.01$, ***$p < 0.001$, ****$p < 0.0001$.

Effects of Orally Administered TNVs on Gut Microbiota and SCFAs in Db/Db Mice

As depicted in Figure 7A, alpha diversity analysis revealed that the richness and diversity of the gut microbiota in *db/db* mice were lower than those in the Control group, which were indicated by the reduced Shannon and Chao1 indices. Compared with the *db/db* group, TNV treatment significantly increased both Shannon and Chao1 indices ($p < 0.01$). Principal component analysis (PCA) demonstrated distinct differences in gut microbiota composition among the Control, *db/db*, and TNV-treated groups ($p < 0.01$) (Figure 7B). Therefore, TNVs can modulate the diversity and composition of the gut microbiota in *db/db* mice. Additionally, the composition of gut microbiota at the *Family, Phylum* and *Genus* levels was further evaluated to investigate the regulatory effect of TNVs on gut microbiota in *db/db* mice. As shown in Figure 7C and D, at the *Family* level, TNV treatment significantly reduced the abundance of harmful bacteria including *Lachnospiraceae* and *Desulfovibrionaceae*, and increased the abundance of *Lactobacillaceae* and *Muribaculaceae*. At the *Phylum* level, TNVs intervention significantly increased the *Bacteroidetes*/*Firmicutes* ratio as well as the abundance of *Proteobacteria* and *Desulfobacterota* (Figure 7G and H). At the *Genus* level, TNVs treatment decreased the relative abundance of *Lachnospiraceae_NK4A 136_group* and increased the abundance of *Lactobacillus* (Figure 7E and F).

To further explore the metabolic pathways regulated by gut microbiota of *db/db* mice a PICRUSt2 functional analysis was conducted to reveal the potential metabolic pathways. It was found that the metabolic function of the gut microbiota in *db/db* mice after treatment with TNVs mainly included four metabolic pathways, namely lipid metabolism, carbohydrate metabolism, energy metabolism, and glycolytic metabolism (Figure 7I). Subsequently, a Spearman correlation analysis on serum biochemical indicators, lipid metabolism genes, and gut microbiota was conducted. As shown in Figure 7J–M, *Propionibacteriaceae, Clostridia_UCG.014, Saccharimonadaceae, Muribaculaceae, Patescibacteria, Actinobacteria, Bacteroides*, and *Candidatus* exhibited positive correlations with UCP1, PGC-1α, and HDL-c, and negative correlations with CD36, FBG, and LDL-c. Therefore, TNVs might exhibit beneficial effects on hepatic lipid metabolism disorder of *db/db* mice by regulating gut microbiota composition.

SCFAs could restore energy balance and exert beneficial effects on liver metabolic function by improving the metabolism of glucose and lipid.[24] In this study, the levels of eleven types of SCFAs (acetic acid, propionic acid, butyric acid, isobutyric acid, valeric acid, isovaleric acid, hexanoic acid, heptanoic acid, octanoic acid, nonanoic acid, and decanoic acid) produced by gut microbiota in mouse feces was measured. As shown in Figure 8, the levels of acetic acid, propionic acid, butyric acid, isobutyric acid, valeric acid, and isovaleric acid were reduced in *db/db* mice compared to the Control group. In contrast, treatment with TNVs increased the levels of four SCFAs (acetic acid, propionic acid, butyric acid, and isovaleric acid).

To further elucidate the relationships among the gut microbiota, gut microbial metabolites (particularly SCFAs), and hepatic metabolites in *db/db* mice, Spearman Correlation Coefficient Analysis was conducted. The correlation analyses between the gut microbiota and SCFAs revealed that six SCFAs (acetic acid, propionic acid, isobutyric acid, butyric acid, isovaleric acid, and valeric acid) exhibited a negative correlation with four gut microbial taxa (*Desulfovibrionaceae, Lachnospiraceae, Desulfobacterota*, and *Firmicutes*) while a positive correlation was observed with seven other gut microbial taxa (*Proteobacteria, Muribaculaceae, Lactobacillaceae, Eubacterium, Bacteroides, Lactobacillus*, and *Actinobacteriota*). Furthermore, the analyses of the correlation between SCFAs and hepatic metabolites demonstrated that six SCFAs (acetic acid, propionic acid, isobutyric acid, butyric acid, isovaleric acid, and valeric acid) displayed a negative correlation with choleric acid, taurochenodesoxycholic acid, benzoic acid, deoxycholic acid, 5-HETE, and taurodeoxycholic acid. Conversely, a positive correlation was observed with Taurine and Taurochenodeoxycholate. Additionally, a correlation analysis between the gut microbiota and hepatic metabolites was conducted as well (See detailed information in Figure S4). Notably, Taurodeoxycholic acid, cholenoic acid, Deoxycholic acid, Cholesterol sulfate, Taurochenodeoxycholate, Tauroursodeoxycholic acid, 5-HETE exhibited a negative correlation with eight gut microbial taxa (*Proteobacteria, Patescibacteria, Campilobacterota, Muribaculaceae, Lactobacillus, Bacteroides, Lactobacillaceae*, and *Saccharimonadaceae*) while a positive correlation was observed with four other gut microbial taxa (*Firmicutes, Desulfobacterota, Lachnospiraceae*, and *Desulfovibrionaceae*). In summary, TNVs could restore the gut microbiota composition with increased production of SCFAs (acetic acid, propionic acid, butyric acid and isovaleric acid), which may lead to down regulation of hepatic bile acid metabolism to ammolite the hepatic steatosis.

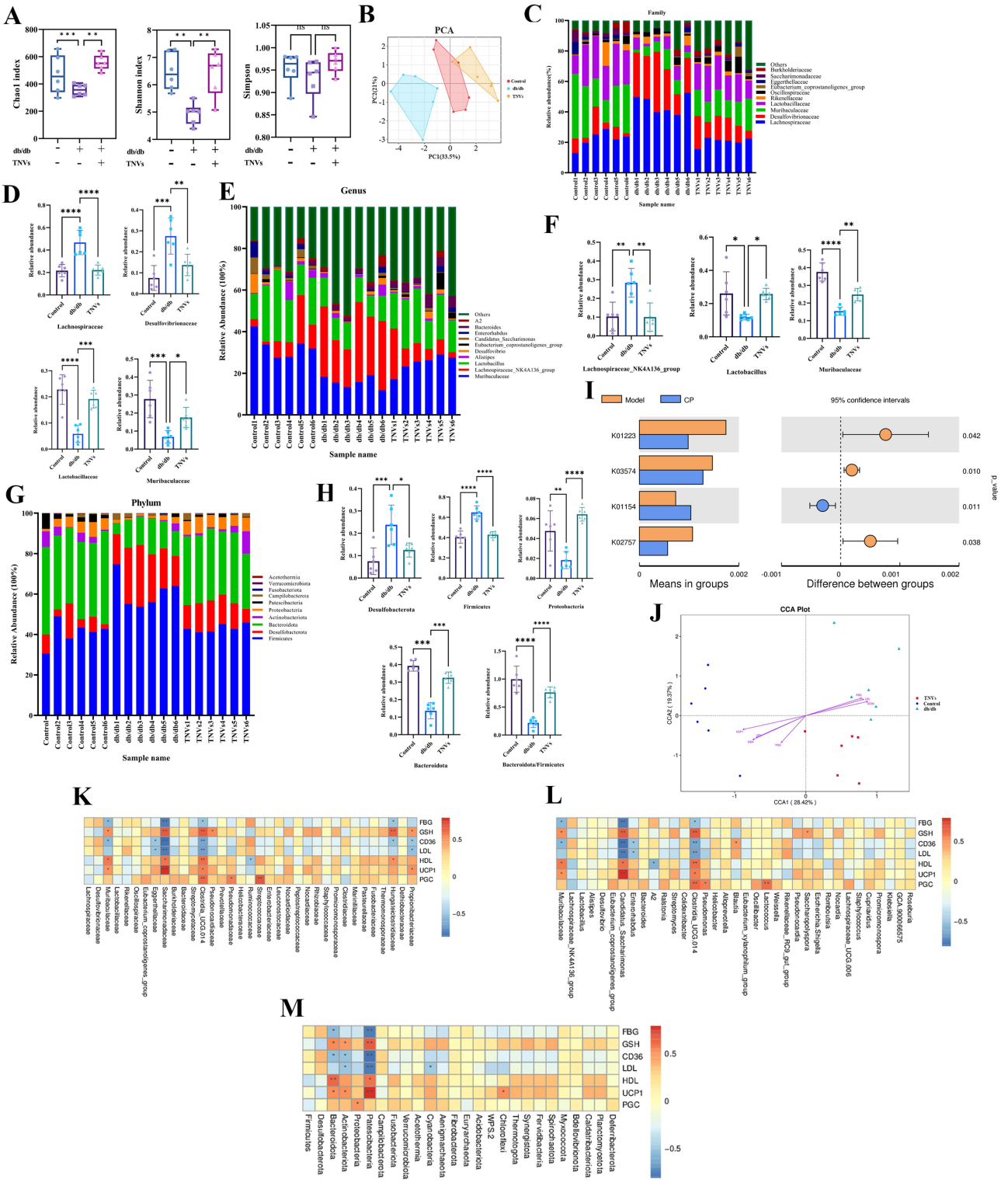

Figure 7 Impact of TNVs on gut microbiota in *db/db* mice. (**A**) Chao1, Shannon, and Simpson indices. (**B**) PCA analysis. (**C**) Relative abundance of bacteria at the family level. (**D**) Representative histogram of gut microbiota composition at the family level. (**E**) Relative abundance of bacteria at the genus level. (**F**) Representative histogram of gut microbiota composition at the genus level. (**G**) Relative abundance of bacteria at the phylum level. (**H**) Representative histogram of gut microbiota composition at the phylum level. (**I**) PICRUSt2 functional annotations of gut microbiota in the Control and *db/db* groups. (**J**) Redundancy analysis (RDA) of gut microbiota and environmental factors. (**K-M**) Heatmaps of Spearman correlation analysis between gut microbiota and environmental factors, where blue represents a negative correlation and red represents a positive correlation.

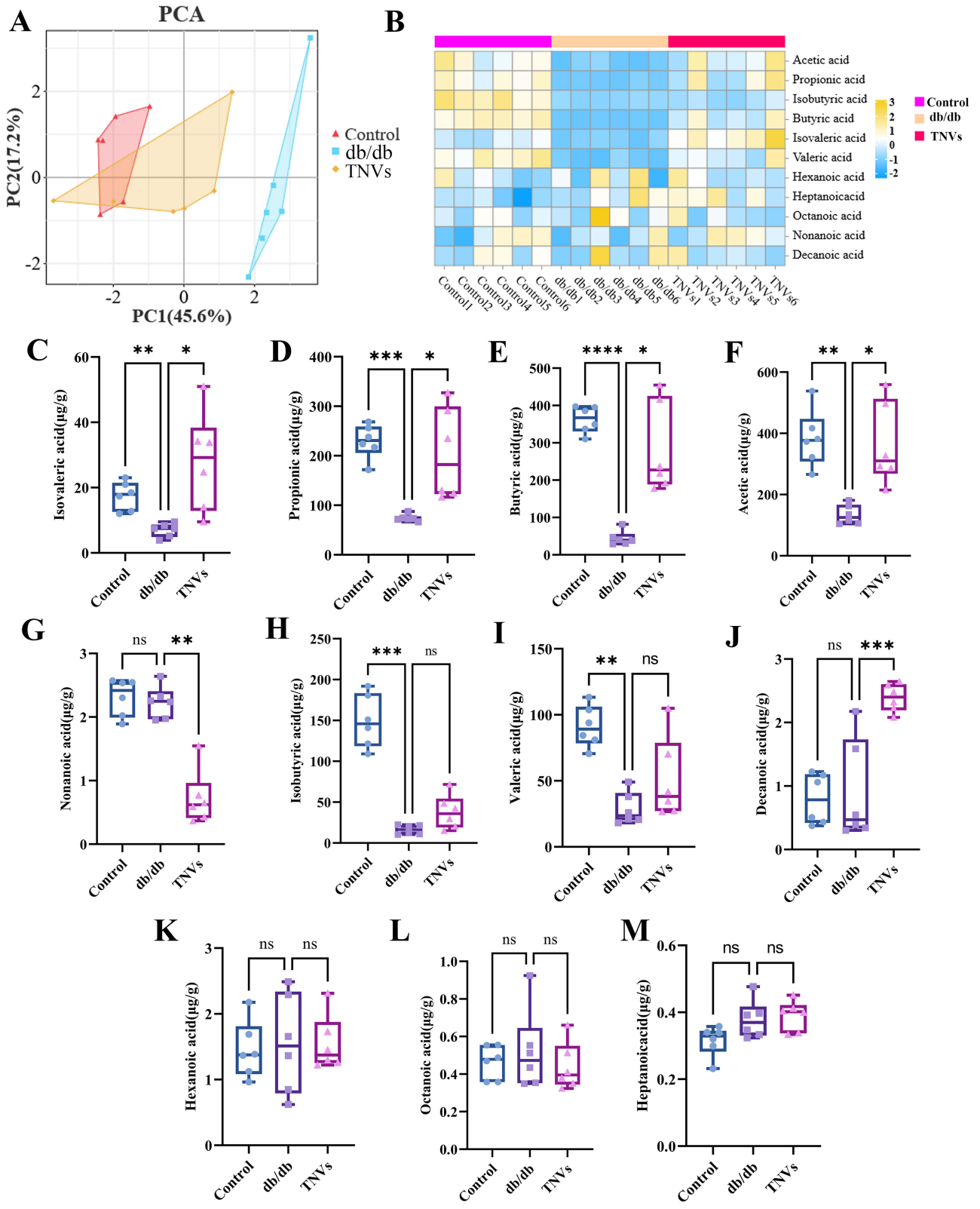

Figure 8 Effect of TNVs on short chain fatty acids in gut microbiota of *db/db* mice. (**A**) Principal component analysis. (**B**) Cluster analysis. (**C**) The levels of isovaleric acid. (**D**) The levels of propionic acid. (**E**) The levels of butyric acid. (**F**) The levels of acetic acid. (**G**) The levels of nonanoic acid. (**H**) The levels of isobutyric acid. (**I**) The levels of valeric acid. (**J**) The levels of decanoic acid. (**K**) The levels of hexanoic acid. (**L**) The levels of octanoic acid. (**M**) The levels of heptanoic acid.

https://doi.org/10.2147/IJN.S478589 DovePress

Discussion

Tangerine peel, a kind of popular function food prepared from *Citrus reticulatae pericarpium*, contains various bioactive compounds including primarily volatile oils, flavonoids, polysaccharides and alkaloids.[5] Bioactive assays for tangerine peel revelated its hepatoprotective,[6] anti-asthmatic, [25] antioxidant,[26] anti-inflammatory[8] and lipid-lowering activities.[5,9,27,28] In the current study, TNVs were isolated from tangerine peel and characterized for the first time. It was found that TNVs contained about 100 bioactive small molecules including flavonoids, alkaloids, phenolic compounds, lipids and amino acids, suggesting our prepared TNVs included numerous bioactive constituents. In addition, zeta potential is a crucial parameter for evaluating the stability of nanoparticle colloids. Typically, nanoparticles with zeta potential values between −30 mV and +30 mV are regarded as having good stability. In our study, the zeta potential of CLDENs in aqueous solution was found to be −12.26 ± 4.05 mV, indicating that the vesicles were stable.

NAFLD is a common metabolic disease with the inhibition on FAO leading to increased glycolysis and lipogenesis in the liver.[29–31] FAO is an important pathway for maintaining energy balance, and PPAR-α, PGC-1α, UCP1, PRDM16, and CPT1/2 are essential genes directly involved in the regulation of fatty acid transport and FAO.[32] Thus, enhancing FAO is crucial for treating hepatic lipid toxicity induced by T2D including NAFLD. In the current study, the downregulated genes for key glycolysis and lipogenesis and upregulated key FAO genes in the liver of *db/db* mice after treatment with TNVs, suggesting that TNVs exhibited the potential to alleviate hepatic steatosis in *db/db* mice possibly by modulating the expression of genes associated with lipid metabolism. The further in vitro AML-12 and 3T3-L1 cells experiments revealed that TNVs inhibited the expression of key lipogenesis genes (SREBP1-c, CD36, ACC, LXR-α, PPAR-γ, CEBPα). Conversely, TNVs increased the expression levels of key fatty acid β-oxidation genes (CPT1, CPT2, FGFR4, PGC-1α, Tmem26, PPAR-α, UCP1, PRDM16). Thus, TNVs protected liver cells from lipid toxicity by promoting fatty acid β-oxidation, inhibiting lipid uptake, glycolysis, and de novo lipogenesis. Furthermore, we observed that TNVs significantly reduced lipid droplet accumulation in AML-12 and 3T3-L1 cells. TNVs also decreased adipocyte hypertrophy and increased lipolysis. Therefore, our findings suggest that TNVs regulate lipid metabolism by downregulating adipogenesis and triglyceride (TG) synthetic genes. This indicates that TNVs can suppress obesity through the browning of white adipose tissue (WAT).

In addition, our results demonstrated TNVs could improve microbial diversity of *db/db* mice. At the family level, TNVs treatment significantly decreased the abundance of harmful bacteria, such as *Lachnospiraceae* and *Desulfovibrionaceae*, and increased the abundance of *Lactobacillaceae* and *Muribaculaceae*. At the genus level, TNVs reduced the relative abundance of *Lachnospiraceae* and increased that of Lactobacillus. At the phylum level, TNVs intervention significantly escalated the abundance of *Proteobacteria* and *Desulfobacterota*, which was supported by the findings of Cui et al.[33] SCFAs, the primary metabolites produced by gut microbiota, was involved in the communication between gut microbial community and the host and further played an important role in the regulation of lipid accumulation, energy homeostasis and hepatic hyperlipidemia.[24] In this study, TNVs treatment not only led to an increase in the biodiversity of gut microbiota but also stimulated the secretion of gut microbiota metabolites including acetic, propionic, isobutyric, butyric, isovaleric and valeric acids. Moreover, the correlation analysis between gut microbiota, SCFAs, and hepatic metabolites revealed that gut microbiota was involved in bile acid metabolism, amino acid metabolism, carbohydrate metabolism, lipid metabolism, energy metabolism, and coenzyme transport metabolism. These findings were particularly pronounced in mice treated with TNVs, which indicated that TNVs can suppress hepatic steatosis in *db/db* mice by modulating gut microbiota.

Metabolomics is a powerful tool for biomarker identification and quantification and enable to acquire a comprehensive metabolomic profile to reveal the potential pathways involving in the therapy. In this study, distinctive metabolic characteristics between Control, *db/db*, and TNVs groups were revealed by untargeted metabolomics analysis with most differential metabolites attributed to metabolic pathways including arachidonic acid metabolism, purine metabolism, glutathione metabolism, primary bile acid biosynthesis, and amino acid metabolism. It has been reported that the metabolism of arachidonic acid (AA) through the cyclooxygenase pathway, lipoxygenases pathway, and cytochrome P450 monooxygenase (CYP450) pathway was closely related to the regulation of hepatic glucose and lipid metabolism homeostasis.[33] Glutathione levels were closely related to glutathione metabolism and its disorder was found to exacerbate liver damage.[24] Excessive biosynthesis of primary bile acid was associated with a series of metabolic disease and inhibiting its excessive biosynthesis could restore the balance of glucose and lipid metabolism.[34]

Besides the above-mentioned therapeutic pathways for metabolic disorders, accumulating evidence has revealed that the beneficial effect of TNVs on metabolic disorders could be achieved by regulation of bile acids through gut microbiota-bile acid-bile acid receptor axis.[35] FXR, the primary bile acid receptor in the liver and small intestine, has a regulatory effect on bile acid synthesis and transport. It also directly or indirectly influences glucose, insulin, lipoprotein, triglyceride, and energy metabolism.[36] Our current study demonstrated that treatment with TNVs could significantly alleviate the excessive biosynthesis of primary/secondary bile acids in *db/db* mice Further mechanistic studies demonstrated that TNVs significantly increased the expression levels of mRNA (FXR, SHP, FGF19, NTCP, HMG-COA, CYP7A1 and β-Klotho) involving in bile acid synthesis and uptake were suppressed by TNVs. Taken together, the above findings provided compelling evidence that TNVs treatment promoted the excretion of bile acids in the liver and reduced bile acid synthesis by activating FXR-FGF pathway and FXR-SHP pathway, respectively, to maintain bile acid homeostasis in the liver, which could serve as a viable therapeutic approach for treating NAFLD induced by T2DM.

Conclusion

It was for the first time found that exosomes isolated from Tangerine peel could alleviate hepatic steatosis induced by T2DM via modulating gut microbiota and enhancing hepatic lipid metabolism. Mechanistic study revealed that TNVs could improve glucose and lipid metabolism by enhancing the expression of genes associated with FAO and inhibiting those associated with lipogenesis and glycolysis in the liver. Additionally, accumulation of cholesterol was inhibited through activating FXR-SHP pathway and promoting the efflux of bile acid in the liver. Moreover, the disordered gut microbiota community of *db/db* mice was restored by TNVs as well.

Acknowledgments

Hong Kong Scholar program and China Postdoctoral Science Foundation; Li Dak Sum Yip Yio Chin R & D Center for Chinese Medicine at The Chinese University of Hong Kong; National & Local Joint Engineering Laboratory of Key Technology & Equipment of Chinese Medicinal Powder at Hunan University of Chinese Medicine. Graphical abstract was created with BioRender.com.

Funding

The research was supported by China Postdoctoral Science Foundation (2021M701180), Hunan University of Chinese Medicine Disciplinary Construction' Revealing the List and Appointing Leaders' Project (22JBZ002), Natural Science Foundation of Hunan Province (2022JJ40322, 2024JJ5303), Hunan Provincial Natural Science Foundation Innovation Research Group Project (2024JJ1007), Science and Technology Planning Project of Outstanding Youth Project of Hunan University of Chinese Medicine (99810001005), General Projects of Hunan Provincial Administration of Traditional Chinese Medicine (B2023013), The Science and Technology Innovation Program of Hunan Province (2023RC3165), National & Local Joint Engineering Laboratory of Key Technology & Equipment of Chinese Medicinal Powder at Hunan University of Chinese Medicine.

Disclosure

The author(s) report no conflicts of interest in this work. The abstract of this paper was presented at the American Association of Pharmaceutical Scientists (AAPS) as an abstract presentation with interim findings. The poster's abstract was published in "Poster Abstracts" in "https://aaps2023.eventscribe.net/fsPopup.asp?PosterID=591227&mode=posterInfo".

References

1. Diaconu CT, Guja C. Nonalcoholic Fatty Liver Disease and Its Complex Relation with Type 2 Diabetes Mellitus-From Prevalence to Diagnostic Approach and Treatment Strategies. *J Clin Med*. 2022;11(17):5144. doi:10.3390/jcm11175144
2. Mantovani A, Petracca G, Beatrice G, Tilg H, Byrne CD, Targher G. Non-alcoholic fatty liver disease and risk of incident diabetes mellitus: an updated meta-analysis of 501 022 adult individuals. *Gut*. 2021;70(5):962–969. doi:10.1136/gutjnl-2020-322572
3. Wu J, Wang K, Wang X, Pang Y, Jiang C. The role of the gut microbiome and its metabolites in metabolic diseases. *Protein Cell*. 2021;12(5):360–373. doi:10.1007/s13238-020-00814-7

4. Wang Y-H. Traditional uses, chemical constituents, pharmacological activities, and toxicological effects of Dendrobium leaves: a review. *J Ethnopharmacol*. 2021;270:113851. doi:10.1016/j.jep.2021.113851
5. Yu X, Sun S, Guo Y, et al. Citri Reticulatae Pericarpium (Chenpi): botany, ethnopharmacology, phytochemistry, and pharmacology of a frequently used traditional Chinese medicine. *J Ethnopharmacol*. 2018;220:265–282. doi:10.1016/j.jep.2018.03.031
6. Wu Y, He Y, Wang R, Zhao X. Preventive Effect of Flavonoid Extract from the Peel of Gonggan (Citrus reticulata Blanco Var. Gonggan) on CCl (4)-Induced Acute Liver Injury in Mice. *J Inflamm Res*. 2021;14:5111–5121. doi:10.2147/JIR.S332134
7. Singh B, Singh JP, Kaur A, Singh N. Phenolic composition, antioxidant potential and health benefits of citrus peel. *Food Res Int*. 2020;132:109114. doi:10.1016/j.foodres.2020.109114
8. Zhang X, Zhou Y, Cheong MS, et al. Citri Reticulatae Pericarpium extract and flavonoids reduce inflammation in RAW 264.7 macrophages by inactivation of MAPK and NF-κB pathways. *Food Front*. 2022;3(4):785–795. doi:10.1002/fft2.169
9. Ling Y, Shi Z, Yang X, et al. Hypolipidemic effect of pure total flavonoids from peel of Citrus (PTFC) on hamsters of hyperlipidemia and its potential mechanism. *Exp Gerontol*. 2020;130:110786. doi:10.1016/j.exger.2019.110786
10. Li A, Wang N, Li N, et al. Modulation effect of chenpi extract on gut microbiota in high-fat diet-induced obese C57BL/6 mice. *J Food Biochem*. 2021;45(4):e13541.
11. Chen XM, Tait AR, Kitts DD. Flavonoid composition of Orange peel and its association with antioxidant and anti-inflammatory activities. *Food Chem*. 2017;218:15–21. doi:10.1016/j.foodchem.2016.09.016
12. Lee GH, Peng C, Park SA, et al. Citrus Peel Extract Ameliorates High-Fat Diet-Induced NAFLD via Activation of AMPK Signaling. *Nutrients*. 2020;12(3).
13. Carvalho BMR, Nascimento LC, Nascimento JC, et al. Citrus Extract as a Perspective for the Control of Dyslipidemia: a Systematic Review With Meta-Analysis From Animal Models to Human Studies. *Front Pharmacol*. 2022;13:822678. doi:10.3389/fphar.2022.822678
14. Zhang X, Gao Z, Yang Y, Pan S, Yin J, Yu X. Rapid identification of the storage age of dried tangerine peel using a hand-held near infrared spectrometer and machine learning. *J Near Infrared Spectrosc*. 2022;30(1):31–39. doi:10.1177/09670335211057232
15. Yi Q, Xu Z, Thakur A, et al. Current understanding of plant-derived exosome-like nanoparticles in regulating the inflammatory response and immune system microenvironment. *Pharmacol Res*. 2023;190:106733. doi:10.1016/j.phrs.2023.106733
16. Hwang JH, Park YS, Kim HS, et al. Yam-derived exosome-like nanovesicles stimulate osteoblast formation and prevent osteoporosis in mice. *J Control Release*. 2023;355:184–198. doi:10.1016/j.jconrel.2023.01.071
17. He C, Wang K, Xia J, et al. Natural exosomes-like nanoparticles in mung bean sprouts possesses anti-diabetic effects via activation of PI3K/Akt/GLUT4/GSK-3β signaling pathway. *J Nanobiotechnology*. 2023;21(1):349. doi:10.1186/s12951-023-02120-w
18. Xu LN, Yin LH, Jin Y, et al. Effect and possible mechanisms of dioscin on ameliorating metabolic glycolipid metabolic disorder in type-2-diabetes. *Phytomedicine*. 2020;67:153139. doi:10.1016/j.phymed.2019.153139
19. Xie G, Wang Y, Wang X, et al. Profiling of serum bile acids in a healthy Chinese population using UPLC-MS/MS. *J Proteome Res*. 2015;14 (2):850–859. doi:10.1021/pr500920q
20. Zou J, Xiang Q, Tan D, et al. Zuogui-Jiangtang-Qinggan-Fang alleviates high-fat diet-induced type 2 diabetes mellitus with non-alcoholic fatty liver disease by modulating gut microbiome-metabolites-short chain fatty acid composition. *Biomed Pharm*. 2023;157:114002. doi:10.1016/j.biopha.2022.114002
21. Song Q, Cheng SW, Li D, et al. Gut microbiota mediated hypoglycemic effect of Astragalus membranaceus polysaccharides in db/db mice. *Front Pharmacol*. 2022;13:1043527. doi:10.3389/fphar.2022.1043527
22. Yu Q, Jiang Z, Zhang L. Bile acid regulation: a novel therapeutic strategy in non-alcoholic fatty liver disease. *Pharmacol Ther*. 2018;190:81–90. doi:10.1016/j.pharmthera.2018.04.005
23. Andrich DE, Melbouci L, Ou Y, et al. A Short-Term High-Fat Diet Alters Glutathione Levels and IL-6 Gene Expression in Oxidative Skeletal Muscles of Young Rats. *Front Physiol*. 2019;10:372. doi:10.3389/fphys.2019.00372
24. Fu M, Zou B, An K, et al. Anti-asthmatic activity of alkaloid compounds from Pericarpium Citri Reticulatae (Citrus reticulata 'Chachi'). *Food Funct*. 2019;10(2):903–911. doi:10.1039/C8FO01753K
25. Wang F, Chen L, Chen S, Chen H, Liu Y. Microbial biotransformation of Pericarpium Citri Reticulatae (PCR) by Aspergillus Niger and effects on antioxidant activity. *Food Sci Nutr*. 2021;9(2):855–865. doi:10.1002/fsn3.2049
26. Wang Y, Zhang X, Zhou C, Khan H, Fu M, Cheang WS. Citri Reticulatae Pericarpium (Chenpi) Protects against Endothelial Dysfunction and Vascular Inflammation in Diabetic Rats. *Nutrients*. 2022;14(24). doi:10.3390/nu14245221
27. Zou J, Wang J, Ye W, et al. Citri Reticulatae Pericarpium (Chenpi): a multi-efficacy pericarp in treating cardiovascular diseases. *Biomed Pharmacother*. 2022;154:113626. doi:10.1016/j.biopha.2022.113626
28. Assini JM, Mulvihill EE, Huff MW. Citrus flavonoids and lipid metabolism. *Curr Opin Lipidol*. 2013;24(1):34–40. doi:10.1097/MOL.0b013e32835c07fd
29. Kim YJ, Choi MS, Woo JT, Jeong MJ, Kim SR, Jung UJ. Long-term dietary supplementation with low-dose nobiletin ameliorates hepatic steatosis, insulin resistance, and inflammation without altering fat mass in diet-induced obesity. *Mol Nutr Food Res*. 2017;61(8). doi:10.1002/mnfr.201600889
30. Guo J, Tao H, Cao Y, Ho C-T, Jin S, Huang Q. Prevention of Obesity and Type 2 Diabetes with Aged Citrus Peel (Chenpi) Extract. *J Agric Food Chem*. 2016;64(10):2053–2061. doi:10.1021/acs.jafc.5b06157
31. Lee K, Lee YJ, Kim KJ, et al. Gomisin N from Schisandra chinensis Ameliorates Lipid Accumulation and Induces a Brown Fat-Like Phenotype through AMP-Activated Protein Kinase in 3T3-L1 Adipocytes. *Int J Mol Sci*. 2020;21(6).
32. Li S, Su W, Zhang XY, Guan YF. Arachidonic acid metabolism in liver glucose and lipid homeostasis. *Sheng Li Xue Bao*. 2021;73(4):657–664.
33. Huang ZR, Chen M, Guo WL, et al. Monascus purpureus-fermented common buckwheat protects against dyslipidemia and non-alcoholic fatty liver disease through the regulation of liver metabolome and intestinal microbiome. *Food Res Int*. 2020;136:109511. doi:10.1016/j.foodres.2020.109511
34. Chiang JYL. Bile acid metabolism and signaling in liver disease and therapy. *Liver Res*. 2017;1(1):3–9. doi:10.1016/j.livres.2017.05.001
35. Boursier J, Mueller O, Barret M, et al. The severity of nonalcoholic fatty liver disease is associated with gut dysbiosis and shift in the metabolic function of the gut microbiota. *Hepatology*. 2016;63(3):764–775. doi:10.1002/hep.28356
36. Loomba R, Seguritan V, Li W, et al. Gut Microbiome-Based Metagenomic Signature for Non-invasive Detection of Advanced Fibrosis in Human Nonalcoholic Fatty Liver Disease. *Cell Metab*. 2019;30(3):607. doi:10.1016/j.cmet.2019.08.002